
KO: Kinetics-inspired Neural Optimizer with PDE Simulation Approaches

Mingquan Feng[†], Yixin Huang[†], Yifan Fu, Shaobo Wang, Junchi Yan^{*}
 Shanghai Jiao Tong University
 yanjunchi@sjtu.edu.cn

Abstract

The design of optimization algorithms for neural networks remains a critical challenge, with most existing methods relying on heuristic adaptations of gradient-based approaches. This paper introduces KO (Kinetics-inspired Optimizer), a novel neural optimizer inspired by kinetic theory and partial differential equation (PDE) simulations. We reimagine the training dynamics of network parameters as the evolution of a particle system governed by kinetic principles, where parameter updates are simulated via a numerical scheme for the Boltzmann transport equation (BTE) that models stochastic particle collisions. This physics-driven approach inherently promotes parameter diversity during optimization, mitigating the phenomenon of parameter condensation, i.e. collapse of network parameters into low-dimensional subspaces, through mechanisms analogous to thermal diffusion in physical systems. We analyze this property, establishing both a mathematical proof and a physical interpretation. Extensive experiments on image classification (CIFAR-10/100, ImageNet) and text classification (IMDB, Snips) tasks demonstrate that KO consistently outperforms baseline optimizers (e.g., Adam, SGD), achieving accuracy improvements while computation cost remains comparable.

1 Introduction

Optimization algorithms are the cornerstone of training modern neural networks, directly influencing model convergence, generalization, and robustness. Gradient-based methods, such as stochastic gradient descent (SGD) [37] and adaptive learning rate optimizers like Adam [21] and AdamW [30], dominate deep learning practice due to their simplicity and empirical efficacy [8, 2, 25]. Concurrently, interdisciplinary efforts have explored physics-inspired optimization paradigms, such as thermodynamic analogies [34] and electromagnetic field [1], which reinterpret network training as energy minimization or dynamical systems. These approaches often borrow conceptual tools from classical mechanics or statistical physics, yet they primarily focus on a gradient-free scheme.

Despite their widespread adoption, conventional optimizers suffer from a critical limitation: they lack mechanisms to systematically regulate the geometric dispersion of network parameters during training. Empirical studies [54, 4] reveal that parameters in over-optimized models often condense into low-dimensional subspaces, a phenomenon termed parameter condensation [48], diminishing representational capacity and exacerbating overfitting. While regularization techniques like weight decay or dropout partially mitigate this issue [53], they act as post hoc corrections rather than addressing the root cause in the optimization dynamics. Furthermore, existing physics-inspired methods often oversimplify the analogy between physical systems and neural networks, neglecting the stochastic, many-body interactions that govern parameter evolution. This gap raises a pivotal

^{*}Correspondence author. Work was in part supported by NSFC (92370201, 62222607).

[†]These authors contributed equally to this work.

question: Can we design optimizers that inherently promote parameter diversity by simulating the microscopic, collision-driven dynamics observed in kinetic systems?

This work introduces KO, a kinetics-inspired neural optimizer that reformulates parameter training as the evolution of a particle system simulated via partial differential equations (PDEs). Drawing parallels between network parameters and particles undergoing elastic collisions, KO employs a numerical discretization of the BTE [3] to model stochastic parameter interactions. This approach naturally enforces parameter dispersion through a thermal diffusion-like mechanism, directly counteracting condensation tendencies. The highlights of this work are threefold:

1. **Physics-Driven optimization framework:** We propose the first optimizer, to our best knowledge, that rigorously integrates kinetic theory and PDE simulation into neural network training, bridging microscopic particle dynamics with macroscopic learning outcomes.
2. **Theoretical and empirical analysis:** We prove that KO’s collision-based updates decrease the weight correlation, and we interpret this behavior by both mathematical and physical analysis.
3. **Empirical performance superiority:** Experiments across image and text classification tasks demonstrate that KO achieves consistent accuracy gains over classical optimizers.

2 Related Work

Deep-learning Gradient-based Optimizers. The evolution of optimization algorithms has been pivotal in advancing deep learning, addressing challenges e.g., convergence speed, stability, and generalization. Early approaches like Stochastic Gradient Descent (SGD) laid the foundation by iteratively updating parameters using gradient directions [38]. Nesterov accelerated gradient [35] introduces momentum, enhancing convergence by incorporating past gradients. The introduction of adaptive learning rates show a shift, with methods like AdaGrad [10], RMSProp [42], Adam optimizer [21] adjusting learning rates based on historical gradients. Second-order methods like BFGS [12] and L-BFGS [27] further improve convergence by approximating the Hessian matrix, though they are computationally expensive for large models. Recent advancements include LAMB [50], which scales learning rates based on layer-wise weight norms, and AdaFactor [40], which reduces memory usage in large models. These developments underscore the ongoing evolution of optimization techniques in deep learning, driven by the need for efficient and effective training methods.

Physics-Inspired Metaheuristics Optimizers. Researchers have taken inspiration from non-linear physical phenomena to formulate meta-heuristic optimization algorithms. For instance, gravitational search algorithms [13, 36] design searcher agents as a collection of masses that interact with each other based on Newtonian gravity and the laws of motion. Likewise, the Electromagnetism-based algorithms [16, 1, 49] define agents as charged particles or electromagnets driven by the electrostatic or magnetic forces. Other metaheuristics include the Fluid Mechanics [9, 41], Optics [19, 18], Thermodynamics [34, 20] and Nuclear physics[44]. These algorithms have been successfully applied to various non-linear optimization problems. However, they are not directly applicable to general deep learning optimization due to the gradient-free nature and lack of a clear connection between the physical process and the gradient-based network optimization dynamics.

3 Methodology

3.1 Preliminaries: Kinetic Theory and Numerical Algorithm

The kinetic molecular theory of ideal gases [29] makes several key assumptions. First, a gas is composed of identical particles called molecules. Second, these molecules are in constant motion, and their behavior can be described using Newton’s laws of motion. Third, the molecules act as small, elastic spheres with negligible volume, meaning the space they occupy is insignificant, and their collisions are perfectly energy-conserving. Lastly, there are no significant attractive or repulsive forces between the molecules.

For systems with an extremely large number of particles, tracking individual trajectories becomes impractical. Instead, we turn to the statistical distributions to describe the system’s dynamics. The change in the number of particles N is hence characterized by f , a density function defined in a 7-dimensional phase space: $dN = f(\mathbf{x}, \mathbf{p}, t) d^3\mathbf{x} d^3\mathbf{p}$. If the displacement \mathbf{x} and momentum \mathbf{p} evolve according to the Hamiltonian equations, and an external force F_{ex} acts on the system, then the density

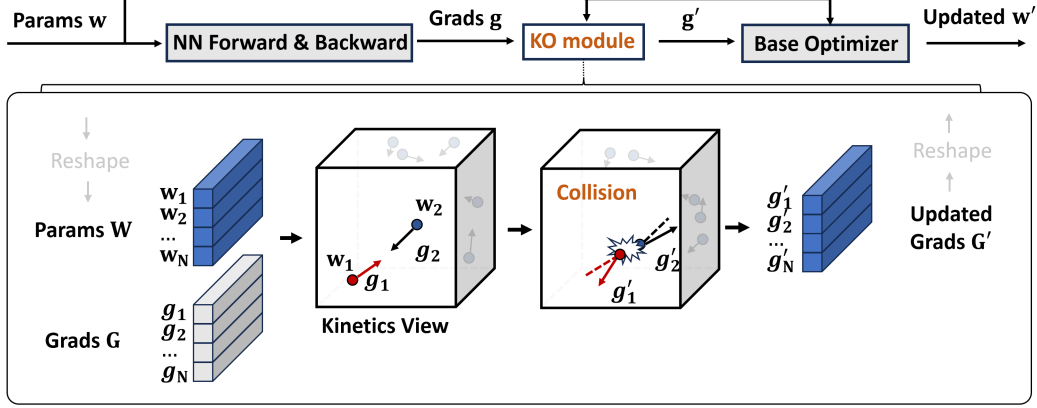


Figure 1: The architecture of KO. The upper part is the workflow of KO composed of a kinetic module and a base optimizer. The gradient is first calculated by network backpropagation, and then updated by the kinetic module, and finally fed into the base optimizer. The lower part is the kinetic module, which simulates the particle collision to update the gradient. The weight and gradient are viewed as the position and velocity of the particles with random collisions. Once two particles collide, the velocity of the particles is updated by the hard-body collision model.

function f obeys the Boltzmann Transport Equation (BTE): $\frac{\partial f}{\partial t} + \frac{\mathbf{p}}{m} \cdot \nabla_{\mathbf{x}} f + F_{ex} \cdot \nabla_{\mathbf{p}} f = \left(\frac{\partial f}{\partial t} \right)_{coll}$, where the right-hand term captures the distribution changes caused by particle collisions, which doesn't have a theoretical formulation and can only be approximated by an empirical formula. As a partial differential equation, BTE governs the temporal evolution of the distribution function f . The Direct Simulation Monte Carlo (DSMC) method [15] and the lattice Boltzmann method [24] are two commonly adopted numerical approaches for solving BTE.

3.2 Direct Simulation Monte Carlo (DSMC)

The DSMC is a stochastic approach that solves BTE for dilute gases by simulating particle motion. In DSMC, each simulation particle represents F_N physical molecules. The method discretizes the computational domain into cells, then tracks particle evolution through drift, wall collision, and particle collision in each cell.

During the drift phase, particles follow straight-line trajectories determined by their current velocities, with the assumption that no collisions occur during this phase. When particles hit domain boundaries, the wall collision step processes these interactions according to the boundary conditions. These two steps provide deterministic updates to the system.

Stochasticity is introduced in the particle collision step. Particle collision only happens between particles that fall into the same cell. The hard sphere model, where the collision probability is proportional to the relative velocity of the particle pairs, is utilized to model the collision:

$$P_{coll}[i, j] = \frac{|\mathbf{v}_i - \mathbf{v}_j|}{\sum_{m=1}^{N_c} \sum_{n=1}^{m-1} |\mathbf{v}_m - \mathbf{v}_n|}, \quad (1)$$

where the N_c is the number of particles in the cell and \mathbf{v} is the particle velocity. The DSMC method utilizes a rejection sampling approach to efficiently approximate collision probabilities, as direct implementation of Eq. 1 would be computationally prohibitive. The algorithm begins by estimating potential collision pairs M_{cand} through the no-time-counter technique: $M_{cand} = \frac{N_c(N_c-1)F_N\pi d^2 v_r^{max}\tau}{2V_c}$, where d is the particle diameter, v_r^{max} is the maximum relative velocity, τ is the time step and V_c is the cell volume. Given this, we can randomly select M_{cand} pairs of candidate particles and determine whether the collision will occur given the following criterion:

$$|\mathbf{v}_i - \mathbf{v}_j|/v_r^{max} > \mathcal{R}_1. \quad (2)$$

where \mathfrak{R}_1 is sampled from the uniform distribution $U(0, 1)$. For accepted collisions, particle velocities are modified according to the chosen collision model while maintaining their spatial positions. This cell-wise procedure iterates until all potential collisions are processed.

The simulation employs the hard sphere collision model, which approximates particles as perfectly rigid bodies. This model strictly conserves both momentum and kinetic energy during collisions while randomizing the scattering direction. Post-collision relative velocities are expressed in the polar coordinate form:

$$\mathbf{v}_r^* = v_r[(\sin \theta \cos \phi)\hat{\mathbf{x}} + (\sin \theta \sin \phi)\hat{\mathbf{y}} + \cos \theta \hat{\mathbf{z}}], \quad (3)$$

where $\phi = 2\pi\mathfrak{R}_2$, $\theta = \cos^{-1}(2\mathfrak{R}_3 - 1)$ and \mathfrak{R}_2 and \mathfrak{R}_3 are numbers randomly sampled from the uniform distribution $U(0, 1)$. If we further denote the center of mass velocity as $\mathbf{v}_{\text{cm}} = (\mathbf{v}_i + \mathbf{v}_j)/2$, then the post-collision velocity can be calculated as:

$$\mathbf{v}_i^* = \mathbf{v}_{\text{cm}} + \mathbf{v}_r^*/2, \mathbf{v}_j^* = \mathbf{v}_{\text{cm}} - \mathbf{v}_r^*/2, \quad (4)$$

3.3 Kinetics-inspired Neural Optimizer

The intuition of the kinetics-inspired neural optimizer is to hinder a phenomenon called the neuron condensation of a neural network [54], where neurons in the same layer cluster together during training. The cosine similarity within the network layer is a key metric to evaluate the degree of condensation. We prove in Section 3.4 that excessive condensation obstructs model performance.

The proposed optimizer architecture is visualized in Fig. 1. Our kinetics-inspired neural optimizer is built on a base optimizer, whether it is an SGD or an Adam optimizer. We apply two different types of collision to the gradients after the backward process to locally update the concerned gradients. Then the optimizer updates the weights according to the base optimizer’s rules. Both types of collision attempt to bring neurons apart to enhance the models’ generalization capacity.

Hard Collision. The hard-body collision is an ideal operation to separate neurons apart. Hard collision updates the gradients by simulating the hard-body collision using the DSMC method. Specifically, the update scheme is detailed as follows:

First, we calculate the relative distance and velocity between neurons, as well as the position and velocity of their center of mass, in order to transform the system into a center-of-mass system:

$$(\mathbf{w}_r)_{i,j} = |\mathbf{w}_i - \mathbf{w}_j|, (\mathbf{g}_r)_{i,j} = |\mathbf{g}_i - \mathbf{g}_j|, (\mathbf{w}_{\text{cm}})_{i,j} = \frac{1}{2}(\mathbf{w}_i + \mathbf{w}_j), (\mathbf{g}_{\text{cm}})_{i,j} = \frac{1}{2}(\mathbf{g}_i + \mathbf{g}_j). \quad (5)$$

Secondly, we derive the formula for the changes of gradients to be applied after the collision, i.e. $\Delta\mathbf{g}$:

$$(\Delta\mathbf{g})_{i,j} = (\mathbf{g}_{\text{cm}})_{i,j} + \frac{1}{2}(g_r)_{i,j}\mathbf{n}_{i,j} - \mathbf{g}_i, \quad (\Delta\mathbf{g})_{j,i} = (\mathbf{g}_{\text{cm}})_{j,i} + \frac{1}{2}(g_r)_{j,i}\mathbf{n}_{j,i} - \mathbf{g}_j, \quad (6)$$

where $\mathbf{n}_{i,j}$ is a unit vector sampled uniformly from the sphere and is uncorrelated with the weight matrix \mathbf{w} , with $\mathbf{n}_{j,i} = -\mathbf{n}_{i,j}$. This formulation extends Eq. 4, in which $(w_r)_{i,j}\mathbf{n}_{i,j}$ and $(w_r)_{j,i}\mathbf{n}_{j,i}$ are derived from Eq. 3 and are used to calculate the post-collision relative receding velocity in the center-of-mass system.

Thirdly, a collision hyperparameter $\text{coll}_{\text{coef}}$ is introduced to control the collision percentage. Unlike traditional DSMC, where collision only happens between particles in the same cell, our method allows collisions between any pair of particles. For each pair of neurons i, j , the collision occurs if:

$$\frac{(g_r)_{i,j} \cdot (U_r)_{i,j}}{g_r^{\text{max}}} > 1 - \text{coll_coef}, \quad (7)$$

where $(U_r)_{i,j} = e^{-(w_r)_{i,j}}$, $g_r^{\text{max}} = \max(g_r)$. This equation is adapted from the original collision filter in Eq. 2. To better control the collision percentage, we further introduce U_r to reflect the effective mean free distance. As the relative distance $(w_r)_{i,j}$ increases, $(U_r)_{i,j}$ decreases, reducing the probability of the collision between neuron i and j .

Finally, we update the gradients of the neurons by the aforementioned collision terms. The update algorithm is summarized in Algorithm 1

$$\mathbf{g}_i^* = \mathbf{g}_i + \sum_{j \text{ in accepted pair } i,j} (\Delta\mathbf{g})_{i,j}, \quad (8)$$

Algorithm 1 Hard Collision Based Gradient Updates

- 1: **Input:** layer weight $\mathbf{w} \in \mathbb{R}^{N \times D}$, layer gradient $\mathbf{g} \in \mathbb{R}^{N \times D}$, hyper-parameters: coll_coef.
 - 2: **Output:** updated layer gradient $\mathbf{g} \in \mathbb{R}^D$.
 - 3: Calculate relative properties $\mathbf{w}_r, \mathbf{g}_r$ and center-of-mass properties $\mathbf{w}_{\text{cm}}, \mathbf{g}_{\text{cm}}$ by Eq. 5;
 - 4: Calculate the full velocity change $\Delta \mathbf{g}$ by Eq. 6;
 - 5: Select collision pairs by Eq. 7;
 - 6: Apply velocity and position change by Eq. 8, get new gradient \mathbf{g} ;
 - 7: **Return** \mathbf{g} ;
-

Algorithm 2 Soft Collision Based Gradient Updates

- 1: **Input:** layer weight $\mathbf{w} \in \mathbb{R}^{N \times D}$, layer gradient $\mathbf{g} \in \mathbb{R}^{N \times D}$, hyper-parameters: coll_coef.
 - 2: **Output:** updated layer gradient $\mathbf{g} \in \mathbb{R}^{N \times D}$.
 - 3: Calculate the repulsion force: $\Delta \mathbf{g} = -\cos(\mathbf{w}, \mathbf{w}) \cos(\mathbf{g}, \mathbf{g}) \mathbf{g}$;
 - 4: Update the gradients: $\mathbf{g} = \mathbf{g} + \text{coll_coef} \Delta \mathbf{g}$;
 - 5: **Return** \mathbf{g} ;
-

Soft Collision. The aim of the kinetics-inspired neural optimizer is to reduce the network layers' weight similarity. Besides directly simulating the collision during the backpropagation, we could artificially design a repulsion force to achieve similar results. Our intuition is to use the gradients and weights at hand to separate neurons.

Intuitively, the higher the similarity, the larger the repulsion force should be. Furthermore, the more positively correlated the neurons are, the more negative the repulsion force should be to push the neurons away. A coefficient matrix that is negatively correlated with the neuron cosine similarity is introduced. We further extend the similarity concept to the gradients. If the gradients aren't correlated, then similarity won't rise. Soft collision is only applied to those neurons with both high weight and gradient similarity. Secondly, we should consider how to formulate the repulsion force. In the gradient descent procedure, the weight moves towards the negative direction of the gradient. If we want a neuron w_i to move in the opposite direction of another neuron w_j , we can just make w_i move in the gradient direction of w_j . The update scheme of soft collision is presented in Algorithm 2.

3.4 Further Understanding of KO from a Mathematical Perspective

In this section, we attempt to provide a mathematical proof of our methods' capacity. Specifically, our method is designed to decrease the weight correlation. Weight correlation is defined as the abstract sum of the network weights' cosine similarity matrix. In fact, [17] states that weight correlation influences models' generalization bounds. The theorem is based on the PAC-Bayesian framework [33], and we can first bound the generalization error w.r.t. the Kullback-Leibler divergence between the posterior and prior distributions of the network parameters [11].

Theorem 3.1 ([11]). *Considering a training dataset S with $m \in \mathbb{N}$ samples drawn from a distribution D . Given a learning algorithm f_Θ with prior and posterior distributions P and Q on the parameters Θ respectively, for any $\delta > 0$, with probability $1 - \delta$ over the draw of training data, we have that*

$$\mathbb{E}_{\Theta \sim Q}[\mathcal{L}_D(f_\Theta)] \leq \mathbb{E}_{\Theta \sim Q}[\mathcal{L}_S(f_\Theta)] + \sqrt{\frac{\text{KL}(Q||P) + \log \frac{m}{\delta}}{2m - 2}} \quad (9)$$

where $\mathbb{E}_{\Theta \sim Q}[\mathcal{L}_D(f_\Theta)]$ is the expected loss on D , $\mathbb{E}_{\Theta \sim Q}[\mathcal{L}_S(f_\Theta)]$ is the empirical loss on S , and their difference yields the generalization error.

[17] further proves the relationship between the generalization error bound and weight correlation.

Theorem 3.2 ([17]). *For a nontrivial network, the decrease in network weight correlation results in the decrease in $\text{KL}(Q||P)$, and further results in the decrease in the upper bound of generalization error introduced in Thm. 3.1.*

We only need to show that our methods contribute to the reduction of weight correlation to prove the capacity. We will show empirically that it results in a decreased weight correlation in the next section. But, firstly, we attempt to give a mathematical justification of our method.

Theorem 3.3. *Given a small enough learning rate, both soft collision and hard collision reduce the weight correlation of the applied network layer.*

The theorem is natural, as our methods artificially provide a force to separate the neurons. The proof is detailed in the Appendix. The collision mechanism is proven to be both mathematically and empirically able to reduce the weight correlation of the network. If we combine the conclusion with Thm. 3.1, we can state that the collision mechanism lowers the models' generalization error.

3.5 Further Understanding of KO from a Physical Perspective

We provide a qualitative explanation from a physical perspective that our collision mechanism can reduce the weight correlation. The collision mechanism is similar to the molecular chaotic collisions in the Boltzmann H-theorem [43]. The Boltzmann H-theorem states that the entropy of a system tends to increase over time, which is a measure of disorder or randomness in a system. In our case, the neurons are analogous to the particles in a gas, and the weight correlation can be interpreted as the order or condensation of the particles. The collision mechanism increases the entropy of the system, which results in a decrease in weight correlation.

To evaluate the relationship between collision and entropy, we first have to define the H quantity, the thermodynamic entropy S .

Definition 3.4 (H quantity). H quantity is defined as:

$$H(t) = \int f(\mathbf{x}, \mathbf{p}, t) \log f(\mathbf{x}, \mathbf{p}, t) d^3\mathbf{x} d^3\mathbf{p} \quad (10)$$

where $f(\mathbf{x}, \mathbf{p}, t)$ is the distribution function of the system in the phase space at time t . The phase consists of position \mathbf{x} and momentum \mathbf{p} of the particles.

Definition 3.5 (Entropy S). The entropy S is a measure of the disorder or randomness in a system and is defined as follows, where k_B is the Boltzmann constant, and Ω is the number of microstates corresponding to a given macrostate.

$$S = k_B \ln \Omega \quad (11)$$

Then we can formulate the relationship between the H quantity and the thermodynamic entropy S in the following lemma.

Lemma 3.6. *For a system of N statistically independent particles, H is related to the thermodynamic entropy S through:*

$$S = -Nk_B H + \text{constant}, \quad (12)$$

Given the aforementioned relationship between H and S , we can interpret changes in the entropy S under collisions using the following H -theorem.

Theorem 3.7 (H -theorem). *Under the molecular chaotic collisions, the H quantity tends to decrease with time to a minimum, while the entropy S increases to a maximum.*

Then we would love to establish a relationship between weight correlation and the entropy of the neuron system. The weight correlation reflects the similarity of neuron weights, which is negatively proportional to the entropy S of weights. Notice that the entropy S is a measure of disorder or randomness in a system, while weight correlation is a measure of order or similarity. The more similar the weights become, the less random the system is, and hence the lower the entropy. For example, if all weights are identical, then the entropy is zero. If the weights are randomly distributed, then the entropy reaches a maximum.

The H -theorem states that the entropy increases with time, which means the weight correlation decreases with time. The collision mechanism in our method is similar to the molecular chaotic collisions in the H -theorem. The collision mechanism increases the entropy of the system, which results in a decrease in weight correlation.

4 Experiments

4.1 Condensation Effects Study

In this section, we validate the anti-condensation effects of the proposed models through experiments. We follow the experiment settings adopted in [55]. We use the cosine similarity of neuron weights to

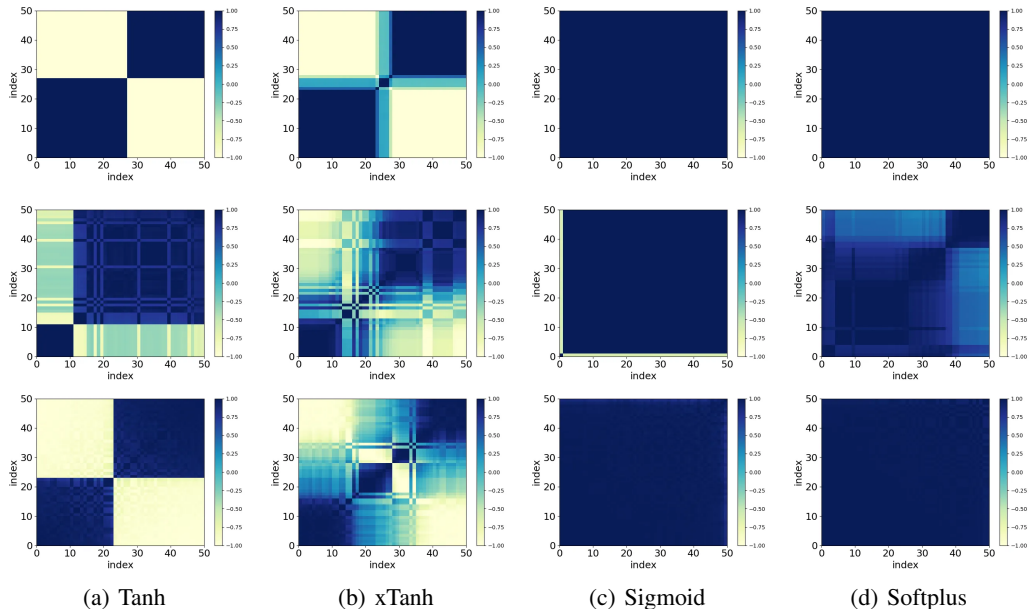


Figure 2: Condensation of two-layer NNs. The color indicates the cosine similarity of two hidden neurons’ input weights at epoch 100, whose indexes are indicated by the abscissa and the ordinate, respectively. The activation functions are indicated by the sub-captions. The first row shows the model weights trained with the original Adam optimizer. The second and third rows depict the results with the Soft Collision and Hard Collision, respectively.

evaluate neuron similarity. The Adam optimizer [22] is adopted on both datasets. We visualize the cosine similarity matrix for better comparison. If neurons are in the same beige (navy blue) block, their input weights have the same (opposite) direction.

Experiments on a Multidimensional Synthetic Dataset Firstly, we perform simple experiments on a multidimensional synthetic dataset. As in [55], we utilize a 2-layer fully-connected network with a hidden dimension 5-50-1 to fit 80 instances sampled from a 5-dimensional function $\sum_{k=1}^5 3.5 \sin(5x_k + 1)$, where each x_k is sampled uniformly from $[-4, 2]$. All parameters are initialized by a Gaussian distribution $\mathcal{N}(0, 0.005^2)$.

The experiment result is shown in Fig. 2. It could be seen that both the proposed hard collision and soft collision hinder the condensation of the weights. The collision makes the network more condensed, and hence, the network could possibly learn more and predict better. As proven previously, this improved condensation will enhance models’ generalization capacity. Our experiment results are in line with the mathematical proof. Further condensation experiments are shown in Appendix B.1. We could draw a simple conclusion in this section that the collision optimizers empirically halt the condensation in the network weights. We shall discuss its influence on model performance in the next section to test our methods’ practicality.

Table 1: Accuracy on CIFAR10 and CIFAR100. The collision is applied to the last fully-connected layer. S.C. is the abbreviation for Soft Collision, and H.C. is the abbreviation for Hard Collision.

Model	CIFAR10	CIFAR100
ResNet18+SGD	95.07%	78.69%
ResNet18+S.C.	95.74%	78.98%
ResNet18+H.C.	95.58%	78.81%
ResNet34+SGD	95.14%	79.42%
ResNet34+S.C.	95.76%	79.78%
ResNet34+H.C.	95.56%	79.53%
ResNet50+SGD	95.37%	78.59%
ResNet50+S.C.	95.83%	79.17%
ResNet50+H.C.	95.57%	78.98%

4.2 Experiments on Image and Text

Experiments on CIFAR-10 and CIFAR-100.

Firstly, we perform experiments on two image datasets, CIFAR-10 and CIFAR-100 [23]. ResNets

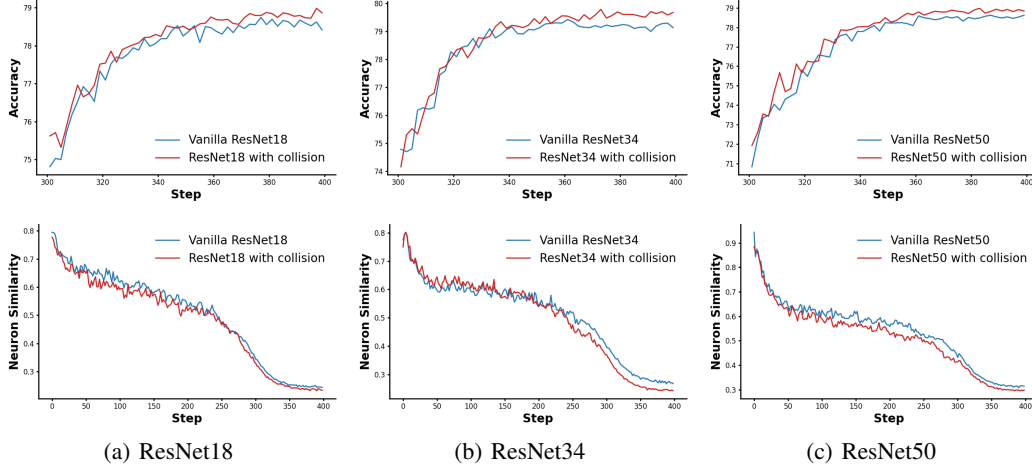


Figure 3: Accuracy and neuron similarity of three different models on CIFAR-100. The upper row shows the test accuracy while the lower row depicts the neuron similarity changes during training.

of various sizes are chosen as the model backbone [14]. A ResNet model can be separated into a convolutional encoder and an FC-layer-based classifier. We apply our proposed collision mechanism to the classifier layer to avoid condensation in that FC layer.

The training process incorporates the SGD optimizer with a weight decay of 5×10^{-4} , a batch size of 128, a momentum of 0.9, and an initial learning rate of 0.1. A Cosine annealing learning rate scheduler is further adopted to better control the learning process. All the models are trained for 200 epochs. Each image is padded by 4 pixels on each side, followed by random cropping of a 32×32 section from the padded image or its horizontal flip, as in the original paper. The prediction accuracy is chosen as the evaluation metric.

Table 1 presents results on CIFAR. The introduction of the collision mechanism boosts the models’ performance. Comparatively, the soft collision improves the test accuracy to a larger extent compared to the hard version. The soft collision approximately increases 0.5% on the test accuracy, while the hard collision raises the accuracy by roughly 0.3%. Furthermore, the incorporation of collision enables shallower models to win over deeper models without collision. On CIFAR-10, ResNet18+Soft Collision predicts better than a vanilla ResNet50. This means that the introduction of this simple optimizer improvement is more effective than merely increasing network depth.

This improvement is notable since the collision mechanism basically introduces no extra time to the training and doesn’t need to modify the model structure, the dataset (no extra augmentation is required), or the training schema. Specifically, it takes 3.68h to train a ResNet50 with the vanilla SGD optimizer and only 3.69h to train a ResNet50 with SGD and Soft Collision. The increase is negligible compared with the entire training duration.

To further show our methods’ influence on the models, we plot the validation accuracy and neuron similarity changes during the training phase in Fig. 3. For simplicity, the neuron similarity is defined as the maximum abstract value in the cosine similarity matrix of the weight matrix. Though this neuron similarity cannot fully represent the similarity situation of the weight matrix, it serves as the upper bound of the similarity level and is still worth evaluating.

Fig. 3 shows that our model can practically help to lower the weight sim-

Table 2: Experimental result on ImageNet-1K. All models are trained and validated at a resolution of 224×224 . The collision is applied to the last fully-connected layer.

Model	T-1 ACC.(%)	T-5 ACC.(%)
ResNet50+Lamb	79.70%	94.53%
ResNet50+S.C.	80.23%	94.79%
ResNet50+H.C.	79.98%	94.61%
ConvNext_Tiny+AdamW	82.10%	96.03%
ConvNext_Tiny+S.C.	82.34%	96.07%
ConvNext_Tiny+H.C.	82.17%	96.03%
ConvNext_Small+AdamW	82.83%	96.29%
ConvNext_Small+S.C.	83.12%	96.33%
ConvNext_Small+H.C.	82.91%	96.29%

ilarity. The incorporation of collision helps to hinder condensation even on this authentic and commonly referred task. The collision mechanism helps the model to maintain a relatively smaller neuron similarity consistently throughout the training. Note our method outperforms the vanilla ResNet model often in the last few epochs of training. It could be attributed to the results of the nature of the cosine annealing learning rate scheduler and the collision.

Experiments on ImageNet-1K In this section, we evaluate our model on a larger image classification dataset, ImageNet-1K [7]. ImageNet-1K includes 1.28 million training images and 50,000 validation images across 1,000 categories. Following a recent paper [46], we adopt a series of data augmentation and regularization strategies, including but not limited to RandAugment [6], Mixup alpha [52], and CutMix alpha [51]. The model training script is based on the timm library [45].

We adopt ResNet and ConvNext [28] as the training backbone. The ResNet 50 training hyperparameters are set as in [46]. We follow the ConvNext hyperparameters as in [26]. For both models, we still only apply collision to the last classifier layer. We evaluate both the Top-1 accuracy and Top-5 accuracy on the models.

Table 2 presents the results of various models on ImageNet-1K. In line with the results in CIFAR-10 and CIFAR-100, the introduction of collision, either the soft version or the hard version, boosts the model performance, both on the Top-1 accuracy and the Top-5 accuracy. The success for both ResNet models and ConvNext shows that our method is not restricted to the ResNet but can be applied to optimize various types of models.

Experiments on IMDB and Snips.

In this section, we attempt to show that our method works not only on image tasks but also on text-related tasks. We choose two simple classification datasets, IMDB [32] and Snips [5]. IMDB comprises 25,000 highly polar movie reviews for training, and 25,000 for testing. Snips is a dataset of over 16,000 crowdsourced queries distributed among seven user intents for intent classification.

As with many text-based tasks, we train a sentiment classifier with a pre-trained backbone. We mainly utilize BERT [8] and DistilBert [39] from the Transformers library by Hugging Face [47]. The classification model consists of a Bert Model transformer with a sequence classification head on top (a fully-connected layer). The collision is applied only to the sequence classification head. Each classification model is trained for 10 epochs using an AdamW optimizer [31].

The results are shown in Table 3. On both of the datasets, collision improves the overall model performance. This result further proves that the collision mechanism works universally. The collision helps with the model regardless of the tasks in concern.

Table 3: Accuracy on the text classification dataset IMDB and Snips with pretrained models. The Soft and Hard Collisions are applied to train the fully-connected layer following the pretrained encoder.

Pretrained Model	IMDB	Snips
bert-base-cased+AdamW	92.52%	98.14%
bert-base-cased+S.C.	93.80%	98.43%
bert-base-cased+H.C.	93.42%	98.43%
bert-base-uncased+AdamW	93.59%	97.71%
bert-base-uncased+S.C.	94.20%	97.89%
bert-base-uncased+H.C.	93.76%	97.73%
distilbert-base-uncased+AdamW	93.07%	97.71%
distilbert-base-uncased+S.C.	93.33%	98.43%
distilbert-base-uncased+H.C.	93.24%	98.11%

5 Conclusion and Limitation Discussion

We have presented KO, a novel neural optimizer that reimagines network parameter training through the lens of kinetic theory and partial differential equation (PDE) simulations. By modeling parameter updates as stochastic collisions in a particle system governed by the BTE, KO introduces a physics-driven mechanism to counteract parameter condensation, a pervasive phenomenon where network parameters collapse into low-dimensional subspaces, impairing model capacity and generalization. Our framework uniquely bridges microscopic kinetic interactions with macroscopic learning dynamics, offering a principled alternative to heuristic, gradient-centric optimization paradigms.

Limitations: computational overhead of simulating collision dynamics, which motivates future research on efficient approximations or hardware-accelerated implementations; extending KO to broader physical systems and analyzing its interplay with modern architectures.

References

- [1] Hosein Abedinpourshotorban, Siti Mariyam Shamsuddin, Zahra Beheshti, and Dayang NA Jawawi. Electromagnetic field optimization: a physics-inspired metaheuristic optimization algorithm. *Swarm and Evolutionary Computation*, 26:8–22, 2016.
- [2] Jinze Bai, Shuai Bai, Yunfei Chu, Zeyu Cui, Kai Dang, Xiaodong Deng, Yang Fan, Wenbin Ge, Yu Han, Fei Huang, et al. Qwen technical report. *arXiv preprint arXiv:2309.16609*, 2023.
- [3] Ludwig Boltzmann. On the relationship between the second fundamental theorem of the mechanical theory of heat and probability calculations regarding the conditions for thermal equilibrium. *Entropy*, 17(4):1971–2009, 2015.
- [4] Zhengan Chen, Yuqing Li, Tao Luo, Zhangchen Zhou, and Zhi-Qin John Xu. Phase diagram of initial condensation for two-layer neural networks. *arXiv preprint arXiv:2303.06561*, 2023.
- [5] Alice Coucke, Alaa Saade, Adrien Ball, Théodore Bluche, Alexandre Caulier, David Leroy, Clément Doumouro, Thibault Gisselbrecht, Francesco Caltagirone, Thibaut Lavril, Maël Primet, and Joseph Dureau. Snips voice platform: an embedded spoken language understanding system for private-by-design voice interfaces, 2018.
- [6] Ekin D. Cubuk, Barret Zoph, Jonathon Shlens, and Quoc V. Le. Randaugment: Practical automated data augmentation with a reduced search space, 2019.
- [7] Jia Deng, Wei Dong, Richard Socher, Li-Jia Li, Kai Li, and Li Fei-Fei. Imagenet: A large-scale hierarchical image database. In *2009 IEEE conference on computer vision and pattern recognition*, pages 248–255. Ieee, 2009.
- [8] Jacob Devlin, Ming-Wei Chang, Kenton Lee, and Kristina Toutanova. Bert: Pre-training of deep bidirectional transformers for language understanding, 2019.
- [9] Berat Doğan and Tamer Ölmez. A new metaheuristic for numerical function optimization: Vortex search algorithm. *Information sciences*, 293:125–145, 2015.
- [10] John Duchi, Elad Hazan, and Yoram Singer. Adaptive subgradient methods for online learning and stochastic optimization. *Journal of machine learning research*, 12(7), 2011.
- [11] Gintare Karolina Dziugaite and Daniel M. Roy. Computing nonvacuous generalization bounds for deep (stochastic) neural networks with many more parameters than training data, 2017.
- [12] Roger Fletcher. *Practical methods of optimization*. John Wiley & Sons, 2000.
- [13] Richard Formato. Central force optimization: a new metaheuristic with applications in applied electromagnetics. *Progress in electromagnetics research*, 77:425–491, 2007.
- [14] Kaiming He, Xiangyu Zhang, Shaoqing Ren, and Jian Sun. Deep residual learning for image recognition, 2015.
- [15] MS Ivanov and SV Rogasinsky. Analysis of numerical techniques of the direct simulation monte carlo method in the rarefied gas dynamics. 1988.
- [16] Behzad Javidy, Abdolreza Hatamlou, and Seyedali Mirjalili. Ions motion algorithm for solving optimization problems. *Applied soft computing*, 32:72–79, 2015.
- [17] Gaojie Jin, Xinpeng Yi, Liang Zhang, Lijun Zhang, Sven Schewe, and Xiaowei Huang. How does weight correlation affect the generalisation ability of deep neural networks, 2020.
- [18] Ali Husseinzadeh Kashan. A new metaheuristic for optimization: optics inspired optimization (oio). *Computers & operations research*, 55:99–125, 2015.
- [19] A Kaveh and M Khayatad. A new meta-heuristic method: ray optimization. *Computers & structures*, 112:283–294, 2012.
- [20] Ali Kaveh and Armin Dadras. A novel meta-heuristic optimization algorithm: thermal exchange optimization. *Advances in engineering software*, 110:69–84, 2017.

- [21] Diederik P Kingma and Jimmy Ba. Adam: A method for stochastic optimization. *arXiv preprint arXiv:1412.6980*, 2014.
- [22] Diederik P. Kingma and Jimmy Ba. Adam: A method for stochastic optimization, 2017.
- [23] Alex Krizhevsky, Geoffrey Hinton, et al. Learning multiple layers of features from tiny images. 2009.
- [24] Timm Krüger, Halim Kusumaatmaja, Alexandr Kuzmin, Orest Shardt, Goncalo Silva, and Erlend Magnus Viggen. The lattice boltzmann method. *Springer International Publishing*, 10(978-3):4–15, 2017.
- [25] Aixin Liu, Bei Feng, Bing Xue, Bingxuan Wang, Bochao Wu, Chengda Lu, Chenggang Zhao, Chengqi Deng, Chenyu Zhang, Chong Ruan, et al. Deepseek-v3 technical report. *arXiv preprint arXiv:2412.19437*, 2024.
- [26] Chongming Liu, Jingyang Ma, Songting Li, and Douglas Zhou. Dendritic integration inspired artificial neural networks capture data correlation. In *The Thirty-eighth Annual Conference on Neural Information Processing Systems*, 2024.
- [27] Dong C Liu and Jorge Nocedal. On the limited memory bfgs method for large scale optimization. *Mathematical programming*, 45(1):503–528, 1989.
- [28] Zhuang Liu, Hanzi Mao, Chao-Yuan Wu, Christoph Feichtenhofer, Trevor Darrell, and Saining Xie. A convnet for the 2020s. In *Proceedings of the IEEE/CVF Conference on Computer Vision and Pattern Recognition (CVPR)*, pages 11976–11986, June 2022.
- [29] Leonard B Loeb. *The kinetic theory of gases*. Courier Corporation, 2004.
- [30] Ilya Loshchilov and Frank Hutter. Decoupled weight decay regularization. *arXiv preprint arXiv:1711.05101*, 2017.
- [31] Ilya Loshchilov and Frank Hutter. Decoupled weight decay regularization, 2019.
- [32] Andrew L. Maas, Raymond E. Daly, Peter T. Pham, Dan Huang, Andrew Y. Ng, and Christopher Potts. Learning word vectors for sentiment analysis. In *Proceedings of the 49th Annual Meeting of the Association for Computational Linguistics: Human Language Technologies*, pages 142–150, Portland, Oregon, USA, June 2011. Association for Computational Linguistics.
- [33] David A. McAllester. Pac-bayesian model averaging. In *Proceedings of the Twelfth Annual Conference on Computational Learning Theory*, COLT '99, page 164–170, New York, NY, USA, 1999. Association for Computing Machinery.
- [34] Sara Moein and Rajasvaran Logeswaran. Kgmo: A swarm optimization algorithm based on the kinetic energy of gas molecules. *Information Sciences*, 275:127–144, 2014.
- [35] Yurii Nesterov. A method for unconstrained convex minimization problem with the rate of convergence $O(1/k^2)$. In *Dokl. Akad. Nauk. SSSR*, volume 269, page 543, 1983.
- [36] Esmat Rashedi, Hossein Nezamabadi-Pour, and Saeid Saryazdi. Gsa: a gravitational search algorithm. *Information sciences*, 179(13):2232–2248, 2009.
- [37] Herbert Robbins and Sutton Monro. A stochastic approximation method. *The annals of mathematical statistics*, pages 400–407, 1951.
- [38] Sebastian Ruder. An overview of gradient descent optimization algorithms. *arXiv preprint arXiv:1609.04747*, 2016.
- [39] Victor Sanh, Lysandre Debut, Julien Chaumond, and Thomas Wolf. Distilbert, a distilled version of bert: smaller, faster, cheaper and lighter, 2020.
- [40] Noam Shazeer and Mitchell Stern. Adafactor: Adaptive learning rates with sublinear memory cost. In *International Conference on Machine Learning*, pages 4596–4604. PMLR, 2018.

- [41] Mojtaba Tahani and Narek Babayan. Flow regime algorithm (fra): a physics-based meta-heuristics algorithm. *Knowledge and Information Systems*, 60:1001–1038, 2019.
- [42] Tijmen Tieleman and Geoffrey Hinton. Lecture 6.5-rmsprop: Divide the gradient by a running average of its recent magnitude. *COURSERA: Neural networks for machine learning*, 4(2):26–31, 2012.
- [43] Richard Chace Tolman. *The principles of statistical mechanics*. Courier Corporation, 1979.
- [44] Zhenglei Wei, Changqiang Huang, Xiaofei Wang, Tong Han, and Yintong Li. Nuclear reaction optimization: A novel and powerful physics-based algorithm for global optimization. *IEEE Access*, 7:66084–66109, 2019.
- [45] Ross Wightman. Pytorch image models. <https://github.com/rwightman/pytorch-image-models>, 2019.
- [46] Ross Wightman, Hugo Touvron, and Hervé Jégou. Resnet strikes back: An improved training procedure in timm, 2021.
- [47] Thomas Wolf, Lysandre Debut, Victor Sanh, Julien Chaumond, Clement Delangue, Anthony Moi, Pierric Cistac, Tim Rault, Rémi Louf, Morgan Funtowicz, Joe Davison, Sam Shleifer, Patrick von Platen, Clara Ma, Yacine Jernite, Julien Plu, Canwen Xu, Teven Le Scao, Sylvain Gugger, Mariama Drame, Quentin Lhoest, and Alexander M. Rush. Huggingface’s transformers: State-of-the-art natural language processing, 2020.
- [48] Zhi-Qin John Xu, Yaoyu Zhang, and Zhangchen Zhou. An overview of condensation phenomenon in deep learning. *arXiv preprint arXiv:2504.09484*, 2025.
- [49] Anupam Yadav et al. Aefa: Artificial electric field algorithm for global optimization. *Swarm and Evolutionary Computation*, 48:93–108, 2019.
- [50] Yang You, Jing Li, Sashank Reddi, Jonathan Hseu, Sanjiv Kumar, Srinadh Bhojanapalli, Xiaodan Song, James Demmel, Kurt Keutzer, and Cho-Jui Hsieh. Large batch optimization for deep learning: Training bert in 76 minutes. *arXiv preprint arXiv:1904.00962*, 2019.
- [51] Sangdoo Yun, Dongyoon Han, Seong Joon Oh, Sanghyuk Chun, Junsuk Choe, and Youngjoon Yoo. Cutmix: Regularization strategy to train strong classifiers with localizable features, 2019.
- [52] Hongyi Zhang, Moustapha Cisse, Yann N. Dauphin, and David Lopez-Paz. mixup: Beyond empirical risk minimization, 2018.
- [53] Zhongwang Zhang and Zhi-Qin John Xu. Implicit regularization of dropout. *IEEE Transactions on Pattern Analysis and Machine Intelligence*, 46(6):4206–4217, 2024.
- [54] Hanxu Zhou, Zhou Qixuan, Tao Luo, Yaoyu Zhang, and Zhi-Qin Xu. Towards understanding the condensation of neural networks at initial training. *Advances in Neural Information Processing Systems*, 35:2184–2196, 2022.
- [55] Hanxu Zhou, Qixuan Zhou, Tao Luo, Yaoyu Zhang, and Zhi-Qin John Xu. Towards understanding the condensation of neural networks at initial training, 2022.

A Proof

Proof of Thm. 3.3. Analyzing the changes in weight correlation of the network layer is equivalent to analyzing the cosine similarity matrix of the layer's weights. We term the weight matrix as w and its i -th and j -th columns as w_i and w_j respectively. Their corresponding gradients are g_i and g_j . After a step of gradient descent, we have:

$$w'_i = w_i - \eta(g_i + \Delta_i), w'_j = w_j - \eta(g_j + \Delta_j) \quad (13)$$

where Δ_i and Δ_j are the collision terms we apply to these two neurons, and η is the learning rate. We will look further into the cosine similarity changes after the gradient descent to prove our methods' capacity. The weight cosine similarity can be calculated as:

$$C = \cos(w_i, w_j) = \frac{w_i^\top w_j}{\|w_i\| \|w_j\|}, C' = \frac{(w_i - \eta(g_i + \Delta_i))^\top (w_j - \eta(g_j + \Delta_j))}{\|w_i - \eta(g_i + \Delta_i)\| \|w_j - \eta(g_j + \Delta_j)\|} \quad (14)$$

We assume that the learning η is a small number. Then we can use Taylor's expansion to get the following results:

$$\begin{aligned} C' &\approx \frac{(w_i^\top w_j - \eta w_i^\top (g_j + \Delta_j) - \eta (g_i + \Delta_i)^\top w_j)(1 + \eta \frac{w_i^\top}{\|w_i\|^2} (g_i + \Delta_i))(1 + \eta \frac{w_j^\top}{\|w_j\|^2} (g_j + \Delta_j))}{\|w_i\| \|w_j\|} \\ &= \frac{w_i^\top w_j (1 + \eta \frac{w_j^\top}{\|w_j\|^2} (g_j + \Delta_j) + \eta \frac{w_i^\top}{\|w_i\|^2} (g_i + \Delta_i)) - \eta w_i^\top (g_j + \Delta_j) - \eta (g_i + \Delta_i)^\top w_j}{\|w_i\| \|w_j\|} \\ &= C + \eta \frac{w_i^\top w_j (\frac{w_j^\top}{\|w_j\|^2} (g_j + \Delta_j) + \frac{w_i^\top}{\|w_i\|^2} (g_i + \Delta_i)) - w_i^\top (g_j + \Delta_j) - (g_i + \Delta_i)^\top w_j}{\|w_i\| \|w_j\|} \\ &= C + \eta \frac{w_i^\top w_j (\frac{w_j^\top}{\|w_j\|} g_j + \frac{w_i^\top}{\|w_i\|} g_i) - w_i^\top g_j - g_i^\top w_j}{\|w_i\| \|w_j\|} \\ &\quad + \eta \frac{w_i^\top w_j (\frac{w_j^\top}{\|w_j\|^2} \Delta_j + \frac{w_i^\top}{\|w_i\|^2} \Delta_i) - w_i^\top \Delta_j - \Delta_i^\top w_j}{\|w_i\| \|w_j\|} \end{aligned} \quad (15)$$

Next, we closely examine the last term in the above equation. The first two terms in Eq. 15 represent the original cosine similarity after the updates. We only need to prove that our collision can hinder condensation on top of the original pipelines.

Soft Collision We first examine the influence of the soft collision. We make a simple assumption that a collision only happens between w_i and w_j . Then we can simplify the collision term to the following format:

$$\Delta_j = \alpha g_i, \Delta_i = \alpha g_j \quad (16)$$

where α is related to the similarity between neurons. We insert this into Eq. 15.

$$\begin{aligned} \delta C &= w_i^\top w_j (\frac{w_j^\top}{\|w_j\|^2} \alpha g_i + \frac{w_i^\top}{\|w_i\|^2} \alpha g_j) - w_i^\top \alpha g_i - \alpha g_j^\top w_j \\ &= \alpha \left[(\cos(w_i, w_j) \frac{\|w_i\|}{\|w_j\|} w_j - w_i)^\top g_i + (\cos(w_i, w_j) \frac{\|w_j\|}{\|w_i\|} w_i - w_j)^\top g_j \right] \end{aligned} \quad (17)$$

For simplicity, we focus on the training phase when it becomes stable; hence, we have $w_i^\top g_i < 0$ and $w_j^\top g_j < 0$. This is because when training is stabilized, g_i won't push w_i too harshly. We find that we can simplify the analysis of the first term in Eq. 17 to determine the sign of $\cos(w_i, w_j) \cos(w_j, g_i) - \cos(w_i, g_i)$ as $\|\frac{w_i}{\|w_j\|} w_j\| = \|w_i\|$. We make an assumption that $\theta(w_i, g_i) < \theta(w_j, g_i)$. The justification of this assumption is that g_i is the gradient of w_i and hence they are more correlated. All the analysis is based on the fact that we only analyze the dynamics in the stable training phase. Then $\cos(w_i, w_j) \cos(w_j, g_i) - \cos(w_i, g_i) < 0$. Since α is negatively correlated with neuron similarity, then δC pushes C in the opposite direction of C and hence lowers the overall cosine similarity. Conclusively, our soft collision helps to lower the overall weight correlation.

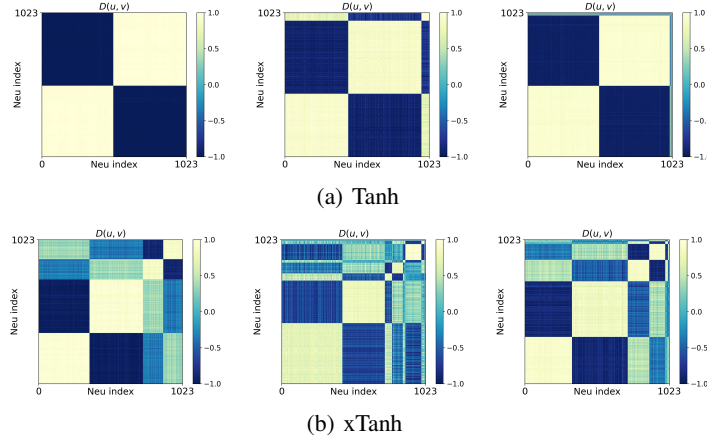


Figure 4: Condensation of Resnet18-like neural networks on CIFAR-10. The color in the figures indicates the cosine similarity of the normalized input weights of two neurons in the first FC layer. The subcaption represents the activation function in the FC layers. The first column shows the model weights trained with the original Adam optimizer. The second and third columns depict the results with the Soft Collision and Hard Collision, respectively.

Hard Collision Next, we analyze how the hard collision functions. In the process of backpropagation, the negative gradient serves as the speed, and the weight matrix serves as the position. The hard collision procedure is detailed in the main paper. We still focus on the single collision between w_i and w_j . The collision term is hence:

$$\Delta_i = \frac{g_j - g_i}{2} + \frac{1}{2}\|g_i - g_j\|u, \Delta_j = \frac{g_i - g_j}{2} - \frac{1}{2}\|g_i - g_j\|u \quad (18)$$

where u is a random vector with no correlation with w . We combine this with Eq. 15:

$$\delta C = (\cos(w_i, w_j) \frac{\|w_i\|}{\|w_j\|} w_j - w_i - \cos(w_i, w_j) \frac{\|w_j\|}{\|w_i\|} w_i + w_j)^\top (\frac{g_i - g_j}{2} - \frac{1}{2}\|g_i - g_j\|u) \quad (19)$$

Since u is a random vector, on average $-\frac{1}{2}\|g_i - g_j\|u$ will not bring any influence to δC . We only need to evaluate the terms that include $\frac{g_j - g_i}{2}$. Another important condition is that the collision only happens when w_i and w_j are close enough and have a large relative speed. This means that $(w_j - w_i)^\top (g_j - g_i) > 0$ and $\cos(w_i, w_j) > 0$. Since the original correlation is positive, we want a $\delta C < 0$ to decrease their weight similarity. Given the above assumption, we can turn to analyze the sign of $(w_j - w_i)^\top (g_i - g_j)$. Given that $(w_j - w_i)^\top (g_j - g_i) > 0$, we have $\delta C < 0$.

Now we have proven that both the soft and hard collision helps to reduce the weight correlation. The theorem gets proven. \square

B Additional Experiments

B.1 Condensation Experiments on CIFAR-10.

We test our methods' anti-condensation effects on a more practical example, CIFAR-10 [23]. We follow the ResNet18-like structure introduced in [55]: the original single fully-connected (FC) layer is replaced with a series of FC layers of size 1024-1024-10. The results are visualized in Fig. 4. The learning rate is 3×10^{-8} for Tanh activation and 5×10^{-6} for xTanh activation. As in the synthetic data experiments, both of the proposed collision methods slow down the original condensation.